

Article

Dimensional Optimization of TiO₂ Nanodisk Photonic Crystals on Lead Iodide (MAPbI₃) Perovskite Solar Cells by Using FDTD Simulations

Lilik Hasanah^{1,*}, Adryan Ashidiq¹, Roer Eka Pawinanto², Budi Mulyanti², Chandra Wulandari^{1,3}, Wiendartun¹ and Ahmad Rifqi Md. Zain⁴

¹ Department of Physics Education, Universitas Pendidikan Indonesia, Bandung 40154, Indonesia; adryan@upi.edu (A.A.); 23320303@mahasiswa.itb.ac.id (C.W.); wien@upi.edu (W.)

² Department of Electrical Engineering Education, Universitas Pendidikan Indonesia, Bandung 40154, Indonesia; roer_eka@upi.edu (R.E.P.); bmulianti@upi.edu (B.M.)

³ Engineering Physics, Institut Teknologi Bandung, Bandung 40132, Indonesia

⁴ Institute of Microengineering and Nanoelectronics (IMEN), Universiti Kebangsaan Malaysia (UKM), Bangi 43600, Selangor, Malaysia; rifqi@ukm.edu.my

* Correspondence: lilikhasanah@upi.edu

Abstract: Perovskite solar cells (PSC) are currently exhibiting reproducible high efficiency, low-cost manufacturing, and scalable electron transport layers (ETL), which are becoming increasingly important. The application of photonic crystals (PC) on solar cells has been proven to enhance light harvesting and lead solar cells to adjust the propagation and distribution of photons. In this paper, the optimization of a two-dimensional nanodisk PC introduced in ETL with an organic-inorganic lead-iodide perovskite (methylammonium lead-iodide, MAPbI₃) as the absorber layer was studied. A finite-difference time-domain (FDTD) simulation was used to evaluate the optical performance of PSC with various lattice constants and a radius of nanodisk photonic crystals. According to the simulation, the optimum lattice constant and PC radius applied to ETL are 500 nm and 225 nm, respectively. This optimum design enhances PSC absorption performance by more than 94% of incident light.

Keywords: perovskite solar cells; 2D photonic crystals; FDTD simulations; nanodisk array



Citation: Hasanah, L.; Ashidiq, A.; Pawinanto, R.E.; Mulyanti, B.; Wulandari, C.; Wiendartun; Md. Zain, A.R. Dimensional Optimization of TiO₂ Nanodisk Photonic Crystals on Lead Iodide (MAPbI₃) Perovskite Solar Cells by Using FDTD Simulations. *Appl. Sci.* **2022**, *12*, 351. <https://doi.org/10.3390/app12010351>

Academic Editors: Filippo Giannazzo and Ivan Shteplyuk

Received: 6 November 2021

Accepted: 20 December 2021

Published: 30 December 2021

Publisher's Note: MDPI stays neutral with regard to jurisdictional claims in published maps and institutional affiliations.



Copyright: © 2021 by the authors. Licensee MDPI, Basel, Switzerland. This article is an open access article distributed under the terms and conditions of the Creative Commons Attribution (CC BY) license (<https://creativecommons.org/licenses/by/4.0/>).

1. Introduction

Perovskite solar cells (PSC) are among the third-generation solar cells in the spotlight because of their rapid efficiency trend and ability to compete with silicon-based solar cells [1]. PSC are solar cells that use the ABX₃ crystal structure, known as the perovskite structure, as an active light-harvesting layer whose solution process uses tin or halides. Perovskite material in solar cells was introduced by Miyasaka et al. in 2009 with an efficiency of 3.8% [2]. Kim et al. (2012) introduced the material N,N-di-p-methoxyphenylamine (or spiro-OMeTAD) as a hole transport layer to improve power conversion efficiency (PCE) [3]. PSC has received much attention because of its cheap materials and fabrication processes, ideal bandgap (1.55 eV), and good efficiency trends [4]. PSC are constantly being improved. In a relatively short period, the highest efficiency achieved in PSC reached 29.40% for the p-type absorber layer made of methylammonium lead-iodide (MAPbI₃) in 2019 [5]. In addition, the MAPbI₃ material in PSC is indeed proven to have high performance [5–9]. In PSC, perovskites act as light absorbers and facilitate the charge transport of electrons. To improve the absorption of perovskite, optical solutions, such as the photonic structure introduced in PSC, can be one of the promising options. Besides increasing the ability to absorb light, the optical solutions also allow a thinner absorber layer [10]. One of the optical solutions mentioned is to apply photonic crystals to the layers of solar cells.

A photonic crystal (PC) is a nanostructure wherein the dielectric constant changes with a period similar to the wavelength of light [11]. PC application to solar cells is

known to maximize light absorption in a particular wavelength range because it has a slow photon effect that increases the interaction of photons and materials [12,13]. PC also has a bandgap, or, specifically, a photonic bandgap (PBG), which is the gap between two adjacent photonic band structures. There are three types of PC based on their spatial arrangement, namely, one-dimensional, two-dimensional, and three-dimensional PC [14]. The higher the dimension, the better the optics enhancement quality. However, the highest dimension of PC (3D) is 1 μm thick instead of in the range of sub-micrometer. Furthermore, it has a complex structure, so the fabrication is more complicated and requires better preparation technologies [15,16].

This study applies a 2D PC in the electron transporting layer (ETL). ETL is a perovskite-coated conductive layer that extracts electrons from the perovskite and carries them to the transparent electrode, resulting in charge recombination [17,18]. The hole transport layer will do the same to the holes as well. Thus, the electron-hole charge recombination can be reduced by utilizing the slow photon effect.

Various types of PC structures have been applied to PSC. Ko et al. have demonstrated this by applying photonic crystals to organic solar cells [19]. There is an increase in light absorption and electrical properties, such as the short circuit current (J_{sc}), fill factor, and open circuit potential (V_{oc}), compared to planar layers. Choi et al. applied nanodisk photonic crystals to ETL and demonstrated greater absorption enhancement and current density than in ETL without photonic crystals [16]. By comparing several studies that applied photonic crystals on PSC to date, it is known that nanodisk photonic crystals with a two-dimensional hexagonal layout design by Choi et al. produce the highest performance [16,20–28]. This work has a similar focus to that of Jeyakumar's et al. study [5]; that is, to study the interface of absorber/ETL. The result shows that their structure provides better performance. The differences between both works are the material used as an absorber layer. Choi et al. use mixed cations and halides perovskite, $(\text{Cs}_x(\text{MA}_{0.17}\text{FA}_{0.83})_{(100-x)}\text{Pb}(\text{I}_{0.83}\text{Br}_{0.17})_3)$, while Jeyakumar et al. use MAPbI_3 [5,16]. Therefore, further study of nanodisk photonic crystals on lead iodide (MAPbI_3) is required to improve the PSC performances.

This study modified the MAPbI_3 PSC using nanodisk PC on titanium dioxide (TiO_2) materials. The geometry of PC, including the lattice constant and radius, is optimized using the finite-difference time-domain (FDTD) method. This optimization was made based on the study of PBG dependence on the PC structure [29]. The PBG changed when the size of the photonic crystal was modified. Furthermore, in this study, variations of the lattice constant and radius of photonic crystal were made to find the optimum PBG. This optimum design can be seen by its optical performance. The optimized performance was determined based on their optical performance. Finally, this study was expected to prove the advantage of PC in the solar cell by providing the enhancement of PSC performance compared to a non-PC structure.

2. Materials and Methods

In this study, simulation is performed in Lumerical FDTD. Various parameters, such as the lattice constant and radius of nanodisk PC were varied. This model structure has five rectangular layers with disk-shaped PC between the absorber/ETL. The layout of this PC is hexagonal because the spacing between unit cells is minimal, which leads to more photons in the slow photon mode [30]. The finite-difference time-domain (FDTD) method is used to simulate the optical properties of the structures made by solving Maxwell's equations. A perfectly matched layer (PML) boundary condition is applied to the top and bottom sides to calculate the absorption spectra in the range of wavelength used in this simulation. In addition, the periodic limits are used on edge boundaries as the periodic 2D PC is introduced in this structure. Furthermore, a plane wave with a 300–1000 nm wavelength range is used as an electromagnetic source.

The material in each PSC layer and the parameters referred to in this study are presented in Table 1. Variation of photonic crystal parameters was selected based on the optimal design of Wang et al. [29]. The material refractive index data for each layer is

obtained from the Palik data [31] for Au layer, from Green et al. [32] for MAPbI₃, from Filipič et al. [33] for Spiro-OmeTAD, and from Raoult et al. [34] for TiO₂. These data will be one of the simulation's inputs, besides the light wavelength range and more previously mentioned conditions.

Table 1. Materials and size parameters for each layer of solar cells used in the simulation. Variations were made on the radius and lattice constant of the PC of TiO₂ nanodisk.

Layer	Material	Size
Transparent Electrode	FTO (fluorine doped tin oxide)	80 nm thick
Electron Transport (ETL)	TiO ₂	100 nm thick
Photonic Crystals	TiO ₂	100 nm thick, 37.5–225 nm radius, 450–1125 nm lattice constant
Perovskite	MAPbI ₃	500 nm
Hole Transport (HTL)	Spiro-OMeTAD	300 nm
Metal Electrode	Au	80 nm

The absorption per unit volume, $A(r, \lambda)$, is obtained using FDTD, and the light absorption is obtained using the Poynting theory, which corresponds to Equation (1) [35]:

$$A(r, \lambda) = \frac{1}{2} \frac{\text{Re}(\vec{\nabla} P)}{P_{in}}$$

$$A(r, \lambda) = \frac{1}{2} \frac{\omega \text{Im}(\epsilon(r, \omega)) |E(r, \omega)|^2}{P_{in}} \quad (1)$$

where E is the electric field, r is position, P_{in} is the incident light source power, ω is the angular frequency, and ϵ is the dielectric constant. The absorption spectra $abs(r, \lambda)$ are obtained by integrating the positions corresponding to Equation (2).

$$abs(r, \lambda) = \int A(r, \lambda) dV \quad (2)$$

with λ is the wavelength of light-source and dV is the volume element.

Then, the photocurrent density (J_{sc}) is obtained from the incident light according to Equation (3).

$$J_{sc} = e \int \frac{\lambda}{hc} abs(\lambda) I_{AM1.5}(\lambda) d\lambda \quad (3)$$

where e is the electron charge, h is Planck's constant, c is the speed of light, and $I_{AM1.5}$ is the 1.5 AM spectrum of solar radiation. This FDTD calculation was performed accurately inside the code of Lumerical FDTD.

3. Results and Discussion

3.1. Structure and Design

The PSC design in this study is simulated to obtain the best performance in terms of the lattice constant and radius of nanodisk variation. Typical structures of PSC include the FTO, ETL, perovskite, HTL, and metal electrode [36]. The simulated structure in this work is presented in Figure 1. The photogenerated charge carriers are generated in the absorber layer and go to the transport layers by the drift process. HTL and ETL block the electrons and holes, respectively, and then collect at the electrodes to create a potential difference. The best material for the absorber layer is methylammonium lead iodide, also known as MAPbI₃, as mentioned in Jeyakumar et al. [5], with efficiency reaching 29%. TiO₂ was commonly used as an ETL because of its proper electronic band levels and ease of fabrication [37]. The other common materials used in PSC was FTO, which is used as a transparent conductive layer, Spiro-OmeTAD was used as HTL, and gold (Au) was used as

a metal electrode layer. The PC structure was introduced to the interface ETL/absorber to enhance the absorption of incident light and increase the interaction between carrier charges with a slow photon effect to reduce the recombination [38]. As with ETL, TiO_2 was used as a PC material. The radius of the nanodisk PC is varied between 37.5 and 225 nm, and the lattice constant is varied between 450 and 1125 nm, while the thickness is fixed at 100 nm. This range is quite representative of finding the optimum size of the photonic crystal and providing a better search for the optimum photonic bandgap, based on the work of Wang et al. [29]. The PC was introduced at ETL/absorber because the energy band alignment at the interface is an essential factor for high-efficiency solar cells [5]. The flat-structured PSC is also simulated to study the enhancement of PSC performance.

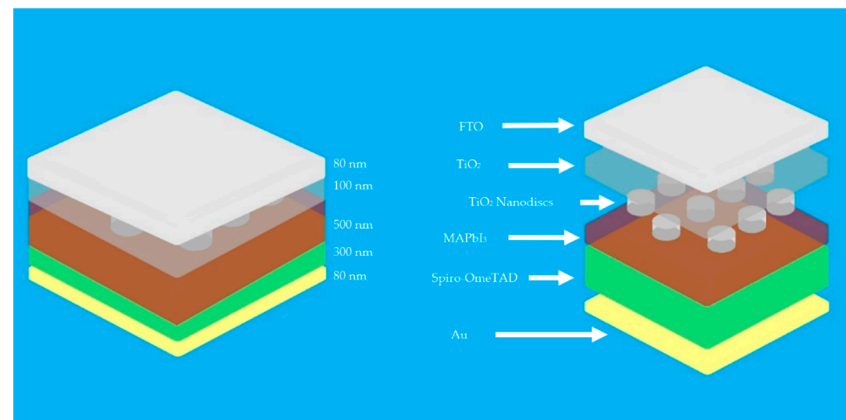


Figure 1. Simulated structures of PSC with photonic crystals on FDTD simulations.

3.2. Optical Performances

The absorption value of PSC is affected by variations in PC radius and lattice constant in the structure. Thus, the contribution of each layer on absorption performance is observed. The absorption spectra of each layer are shown in Figure 2. It can be seen that the perovskite layer (MAPbI_3) contributes the most absorption compared to other layers. This indicates that the function of the perovskite layer as an active layer/absorber works well. This layer absorbed more than 80% of the incident light at 300–630 nm, with the maximum absorption reaching 92% at 409–429 nm of wavelength and dropping at 630–1000 nm. Meanwhile, in the FTO, TiO_2 , Spiro-OMeTAD, and Au layers, it is seen that photons are absorbed much less than in the perovskite layers.

This indicates that only a tiny fraction of the incident light photons is trapped in these layers. Most of the photons are transmitted to the perovskite layer. Figure 3 shows the absorption spectra for all PC radius variations and the lattice constant obtained from the FDTD simulations. It shows the absorption as a wavelength function in the 300–1000 nm range and shows a significant change in absorption for each wavelength point. From 300 nm to 800 nm, the absorption increases as the radius of the nanodisk is higher. It occurs because the more the radius increases, the more that the photons from incident light can be in slow photon mode. On the other hand, the absorption decreases as the lattice constant increases. This also happens because the more lattice constant increase (more space at the structure), the fewer photons get into slow photon mode. The design shows that the structure absorbs over 90% of the incident light. The result proves that the nanodisk PC increases the absorption of the PSC. The optimum performance is achieved at a 225 nm radius of the nanodisk PC, reaching 94% absorption of the incident light, meaning that there is an enhancement of absorption when the flat PSC only reaches 85% at the same wavelength. Figure 4 compares PSC with PC and flat PSC in absorption performance. It shows that there is absorption enhancement in PSC with PC. This enhancement can lead PSC to better electrical performance.

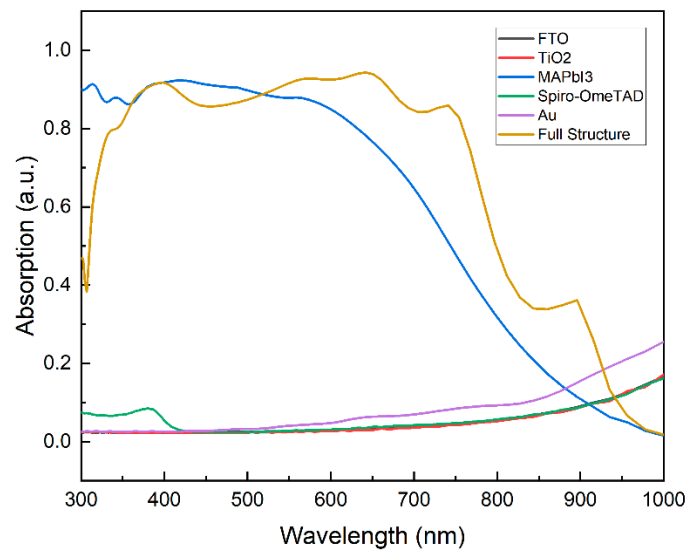


Figure 2. The absorption spectra for every layer in this structure.

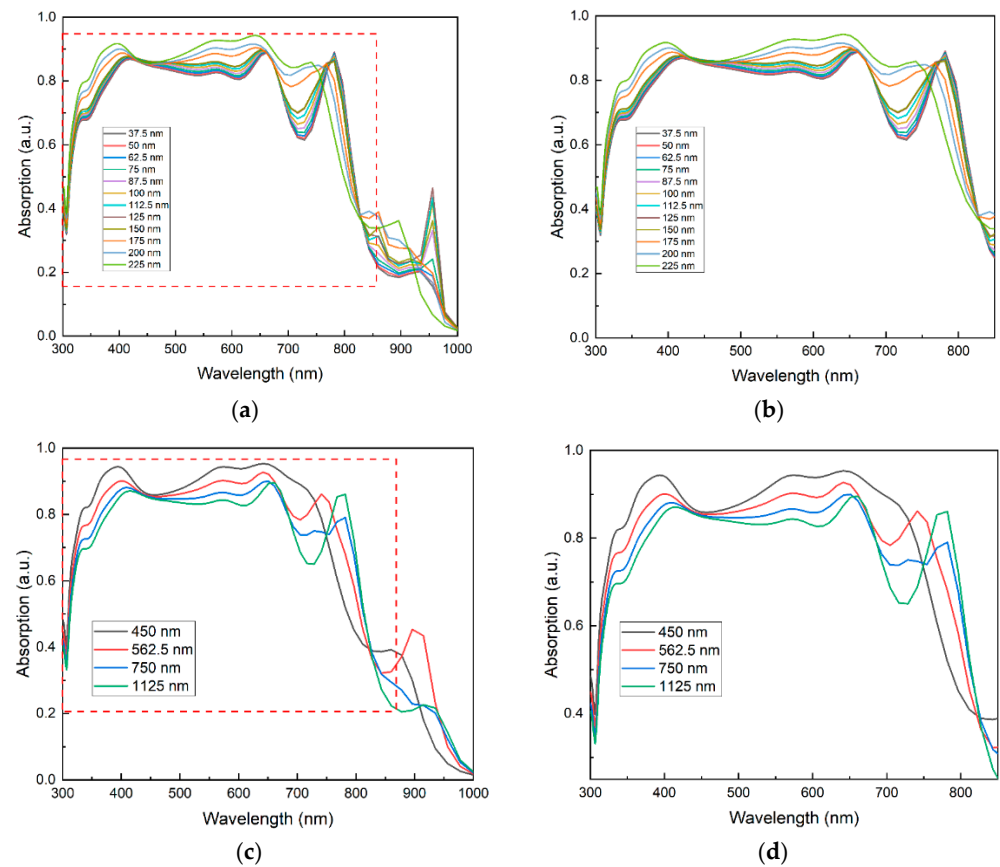


Figure 3. The absorption spectrum profile of PSC for (a) different radius of photonic crystals and (b) enlarged absorption spectrum at 300 nm to 850 nm, and (c) different lattice constant and (d) its enlarged absorption spectrum at 300 nm to 850 nm.

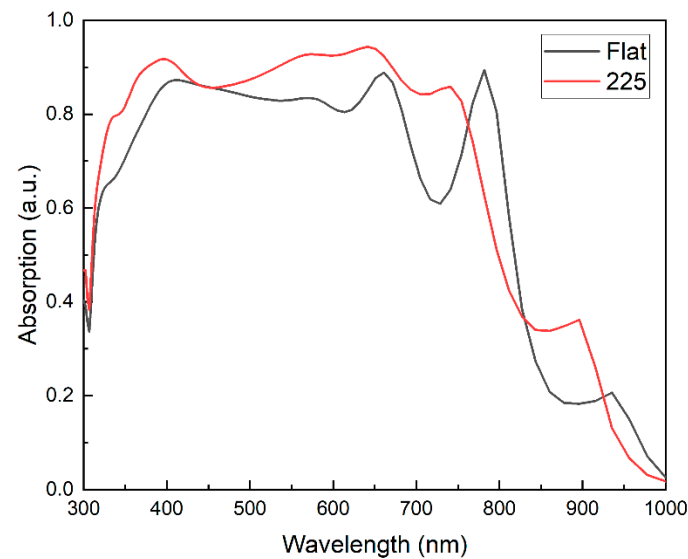


Figure 4. Absorption spectra for PSC without (flat) and with 225 nm radius of nanodisk photonic crystals. The photonic crystals lead to the absorption enhancement of PSC.

Figure 5 shows the distribution profile of electromagnetic wave fields for flat PSC and nanodisk PC-based PSC on every peak of absorption spectra that shown. The profile is analyzed from every peak on absorption spectra, including 390 nm, 642 nm, 759 nm, and 900 nm of optimum design, 225 nm of radius, and 500 nm of lattice constant, as shown in Figure 5. The deep blue color indicates the low-intensity electromagnetic field, while the red color indicates the high-intensity electromagnetic field based on the number above the scale. It is shown in Figure 5 that the electromagnetic field is more likely to be trapped outside the absorber layer for lower wavelength until the wavelength is increased. For a longer wavelength, it starts to enter the absorber layer. From Figure 5, we can also see that the PC-based PSC has a higher electromagnetic field intensity. Moreover, the performance of the PSC is evaluated by its J_{sc} , and it is shown in Table 2. The trends of J_{sc} are linear to the result of absorption spectra. The highest J_{sc} that reached by the optimum design ($r = 225$ nm, $a = 500$ nm) in this work is 26.473 mA/cm². This result also proves that when the absorber material used is MAPbI₃; the performance is increased compared to the work by Choi et al. [16]. Another comparison from previous work is presented in Table 3. This work provides a higher optical performance among other applications of PC on PSC. The comparison is given in terms of the specific wavelength that is 446 nm, where the solar spectrum $I_{AM1.5}$ has a high intensity [39].

Table 2. The photocurrent density (J_{sc}) for certain variations of the radius (r) and lattice constant (a) of PC and flat PSC in this work.

r (nm)	a (nm)	J_{sc} (mA/cm ²)
(Flat PSC)	(Flat PSC)	24.470
50	500	24.659
100		25.428
150		26.153
200		26.467
225		26.473
225	450	26.251
	562.5	26.187
	750	25.220
	1125	24.618

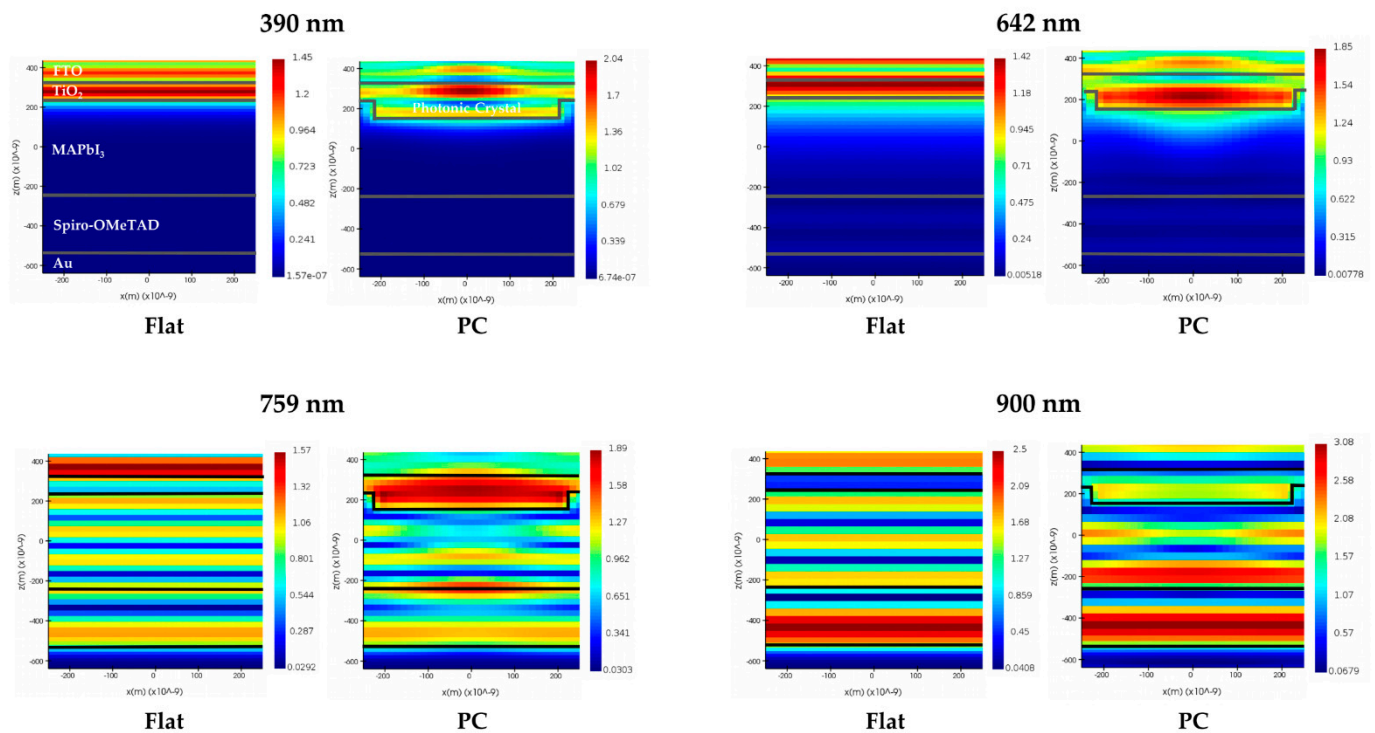


Figure 5. Electromagnetic field density profile of flat and PC-based PSC in 390 nm, 642 nm, 759 nm, and 900 nm.

Table 3. The comparison of optical performance in this work with previous studies about application of PC on PSC at 446 nm of wavelength.

Structure	PC Shape	Absorption	J_{sc} (mA/cm ²)	Reference
FTO/TiO ₂ /MAPbI _{3-x} Cl _x /Spiro-OmeTAD	Inverse Opal	55%	17.1	[40]
FTO/TiO ₂ /MAPbI ₃ /Spiro-OmeTAD	Nanorod	57%	19.18	[41]
FTO/TiO ₂ /MAPbI ₃ /Spiro-OmeTAD	Inverse Opal	72%	14.9	[42]
FTO/TiO ₂ /MAPbI ₃ /Spiro-OmeTAD	Hemisphere	82%	26.5	[22]
FTO/TiO ₂ /MAPbI ₃ /Spiro-OmeTAD	Nanodisk	87%	26.5	This work

4. Conclusions

This work successfully obtained the optimum design of 2D nanodisk hexagonal photonic crystals for PSC application using the FDTD method. The radius of photonic crystals has been varied from 37.5–225 nm, and the lattice constant is varied from 450–1125 nm. The results show that the nanodisk PC with 225 nm of radius and 500 nm of lattice constant provides the highest absorption, with up to 94% of the incident light absorbed. It also gives the highest J_{sc} , which is 26.473 mA/cm². From this work, it is known that when the radius of nanodisk PC increases, the absorption also increases. This occurs because the larger the PC radius, the more photon from the incident light can be in slow photon mode. On the other hand, when the lattice constant is increased, the absorption is decreased due to larger spacing on the structure so that the photon that moves into slow photon mode is fewer. It is best to keep the spacing of the photonic crystal at a minimum and the surface area of the photonic crystal larger to achieve the photon being in slow photon mode. The application of nanodisk photonic crystals in PSC is proven to enhance the absorption higher than that of the flat PSC. This study proved that the PC is advantageous for optimizing solar cell performance. Further study will simulate the electrical properties of the proposed design as a preliminary study for the actual application of solar cells.

Author Contributions: L.H., A.A., provided the conceptualization, original draft, investigation, and formal analysis; C.W. provided methodology, data curation, and investigation; R.E.P. and W. provided validation, article review and editing; A.R.M.Z. provided validation and software; B.M. provided validation provided funding acquisition and supervised the project. All authors have read and agreed to the published version of the manuscript.

Funding: This research was supported by funding from the Ministry of Education, Culture, Research, and Technology, Republic of Indonesia with grant 276/UN40.LP/PT.01.03/2021 and World Class University Program from Universitas Pendidikan Indonesia.

Acknowledgments: The authors thank Universitas Pendidikan Indonesia for providing the facility and supports for conducting progress meetings. Also, the Institute of Microengineering and Nanoelectronics (IMEN), Universiti Kebangsaan Malaysia for giving access to the license of Lumerical software.

Conflicts of Interest: The authors declare that there are no conflict of interest regarding the publication of this paper.

References

1. Yan, J.; Saunders, B. Third-generation solar cells: A review and comparison of polymer: Fullerene, hybrid polymer and perovskite solar cells. *RSC Adv.* **2014**, *4*, 43286–43314. [[CrossRef](#)]
2. Kojima, A.; Teshima, K.; Shirai, Y.; Miyasaka, T. Organometal Halide Perovskites as Visible-Light Sensitizers for Photovoltaic Cells. *J. Am. Chem. Soc.* **2009**, *131*, 6050–6051. [[CrossRef](#)] [[PubMed](#)]
3. Kim, H.-S.; Lee, C.-R.; Im, J.-H.; Lee, K.-B.; Moehl, T.; Marchioro, A.; Moon, S.-J.; Humphry-Baker, R.; Yum, J.-H.; Moser, J.E.; et al. Lead Iodide Perovskite Sensitized All-Solid-State Submicron Thin Film Mesoscopic Solar Cell with Efficiency Exceeding 9%. *Sci. Rep.* **2012**, *2*, 591. [[CrossRef](#)] [[PubMed](#)]
4. Sahoo, S.K.; Manoharan, B.; Sivakumar, N. Introduction: Why perovskite and perovskite solar cells? In *Perovskite Photovoltaics*; Academic Press: Cambridge, MA, USA, 2018.
5. Jeyakumar, R.; Bag, A.; Nekovei, R.; Radhakrishnan, R. Interface studies by simulation on methylammonium lead iodide based planar perovskite solar cells for high efficiency. *Sol. Energy* **2019**, *190*, 104–111. [[CrossRef](#)]
6. Tseng, C.-C.; Chen, L.-C.; Chang, L.-B.; Wu, G.-M.; Feng, W.-S.; Jeng, M.-J.; Chen, D.W.; Lee, K.-L. Cu₂O-HTM/SiO₂-ETM assisted for synthesis engineering improving efficiency and stability with heterojunction planar perovskite thin-film solar cells. *Sol. Energy* **2020**, *204*, 270–279. [[CrossRef](#)]
7. Singh, N.; Agarwal, A.; Agarwal, M. Numerical simulation of highly efficient lead-free perovskite layers for the application of all-perovskite multi-junction solar cell. *Superlattices Microstruct.* **2021**, *149*, 106750. [[CrossRef](#)]
8. Badrooj, M.; Jamali-Sheini, F.; Torabi, N. Roles of Sn content in physical features and charge transportation mechanism of Pb-Sn binary perovskite solar cells. *Sol. Energy* **2020**, *209*, 590–601. [[CrossRef](#)]
9. Shahverdi, N.; Yaghoubi, M.; Goodarzi, M.; Soleamani, A. Optimization of anti-reflection layer and back contact of Perovskite solar cell. *Sol. Energy* **2019**, *189*, 111–119. [[CrossRef](#)]
10. Haque, S.; Mendes, M.J.; Sanchez-Sobrado, O.; Águas, H.; Fortunato, E.; Martins, R. Photonic-structured TiO₂ for high-efficiency, flexible and stable Perovskite solar cells. *Nano Energy* **2019**, *59*, 91–101. [[CrossRef](#)]
11. Shelby, R.A.; Smith, D.R.; Schultz, S. Experimental Verification of a Negative Index of Refraction. *Science* **2001**, *292*, 77–79. [[CrossRef](#)]
12. Baba, T. Slow light in photonic crystals. *Nat. Photonics* **2008**, *2*, 465–473. [[CrossRef](#)]
13. Chen, J.I.L.; von Freymann, G.; Choi, S.Y.; Kitaev, V.; Ozin, G.A. Slow photons in the fast lane in chemistry. *J. Mater. Chem.* **2008**, *18*, 369–373. [[CrossRef](#)]
14. John, S. Light trapping and solar energy harvesting with 3D photonic crystals. In Proceedings of the IEEE Photonics Conference 2012, Burlingame, CA, USA, 23–27 September 2012; Volume 3, p. 126. [[CrossRef](#)]
15. Zhenhua, W. Back Reflector of Solar Cells Consisting of One-dimensional Photonic Crystal and Double-layered Two-dimensional Photonic Crystal. *Acta Photonica Sin.* **2016**, *45*, 223003. [[CrossRef](#)]
16. Choi, D.H.; Nam, S.K.; Jung, K.; Moon, J.H. 2D photonic crystal nanodisk array as electron transport layer for highly efficient perovskite solar cells. *Nano Energy* **2019**, *56*, 365–372. [[CrossRef](#)]
17. Yang, D.; Zhou, X.; Yang, R.; Yang, Z.; Yu, W.; Wang, X.; Li, C.; Liu, S.; Liu, S. (Frank); Chang, R.P.H. Surface optimization to eliminate hysteresis for record efficiency planar perovskite solar cells. *Energy Environ. Sci.* **2016**, *9*, 3071–3078. [[CrossRef](#)]
18. Choi, J.; Song, S.; Hörantner, M.T.; Snaith, H.; Park, T. Well-Defined Nanostructured, Single-Crystalline TiO₂ Electron Transport Layer for Efficient Planar Perovskite Solar Cells. *ACS Nano* **2016**, *10*, 6029–6036. [[CrossRef](#)] [[PubMed](#)]
19. Ko, D.-H.; Tumbleston, J.R.; Zhang, L.; Williams, S.; DeSimone, J.M.; Lopez, R.; Samulski, E.T. Photonic Crystal Geometry for Organic Solar Cells. *Nano Lett.* **2009**, *9*, 2742–2746. [[CrossRef](#)]
20. Zhangyang, X.; Liu, L.; Lv, Z.; Lu, F.; Tian, J. Comparative analysis of light trapping GaN nanohole and nanorod arrays for UV detectors. *J. Nanopart. Res.* **2020**, *22*, 1–10. [[CrossRef](#)]

21. De Zoysa, M.; Ishizaki, K.; Tanaka, Y.; Sai, H.; Matsubara, K.; Noda, S. Enhanced efficiency of ultrathin (~500 nm)-film microcrystalline silicon photonic crystal solar cells. *Appl. Phys. Express* **2016**, *10*, 012302. [[CrossRef](#)]
22. Kim, D.I.; Lee, J.W.; Jeong, R.H.; Yu, J.-H.; Yang, J.W.; Nam, S.-H.; Boo, J.-H. Enhancing the optical properties using hemisphere TiO₂ photonic crystal as the electron acceptor for perovskite solar cell. *Appl. Surf. Sci.* **2019**, *487*, 409–415. [[CrossRef](#)]
23. Liu, Z.; Wu, L.; Wang, X.; Xu, Q.; Hu, Y.; Meng, K.; Chen, G. Improving efficiency and stability of colorful perovskite solar cells with two-dimensional photonic crystals. *Nanoscale* **2020**, *12*, 8425–8431. [[CrossRef](#)]
24. Ramos, F.J.; Oliva-Ramírez, M.; Nazeeruddin, M.K.; Graetzel, M.; González-Elipe, A.R.; Ahmad, S. Light management: Porous 1-dimensional nanocolumnar structures as effective photonic crystals for perovskite solar cells. *J. Mater. Chem. A* **2016**, *4*, 4962–4970. [[CrossRef](#)]
25. Du, Q.G.; Shen, G.; John, S. Light-trapping in perovskite solar cells. *AIP Adv.* **2016**, *6*, 065002. [[CrossRef](#)]
26. Tavakoli, M.M.; Tsui, K.H.; Zhang, Q.; He, J.; Yao, Y.; Li, D.; Fan, Z. Highly Efficient Flexible Perovskite Solar Cells with Antireflection and Self-Cleaning Nanostructures. *ACS Nano* **2015**, *9*, 10287–10295. [[CrossRef](#)] [[PubMed](#)]
27. Zhang, W.; Anaya, M.; Lozano, G.; Calvo, M.E.; Johnston, M.B.; Míguez, H.; Snaith, H.J. Highly Efficient Perovskite Solar Cells with Tunable Structural Color. *Nano Lett.* **2015**, *15*, 1698–1702. [[CrossRef](#)] [[PubMed](#)]
28. Kang, S.M.; Jang, S.; Lee, J.-K.; Yoon, J.; Yoo, D.-E.; Lee, J.-W.; Choi, M.; Park, N.-G. Moth-Eye TiO₂ Layer for Improving Light Harvesting Efficiency in Perovskite Solar Cells. *Small* **2016**, *12*, 2443–2449. [[CrossRef](#)]
29. Wang, X.; Fujimaki, M.; Awazu, K. Photonic crystal structures in titanium dioxide (TiO₂) and their optimal design. *Opt. Express* **2005**, *13*, 1486–1497. [[CrossRef](#)]
30. Gwomei, W.U.; Ju, N.T.; Chang, T.W.; Feng, W.S. Study of two-dimensional photonic crystal arrays for beam splitters. *Mater. Sci.* **2016**, *22*, 218–222. [[CrossRef](#)]
31. Palik, E.D. *Handbook of Optical Constants of Solids*; Academic Press: Cambridge, MA, USA, 2008.
32. Green, M.A.; Jiang, Y.; Soufiani, A.M.; Ho-Baillie, A. Optical Properties of Photovoltaic Organic–Inorganic Lead Halide Perovskites. *J. Phys. Chem. Lett.* **2015**, *6*, 4774–4785. [[CrossRef](#)]
33. Filipič, M.; Loeper, P.; Niesen, B.; De Wolf, S.; Krč, J.; Ballif, C.; Topic, M. CH₃NH₃PbI₃ perovskite / silicon tandem solar cells: Characterization based optical simulations. *Opt. Express* **2015**, *23*, A263–A278. [[CrossRef](#)]
34. Raoult, E.; Bodeux, R.; Jutteau, S.; Rives, S.; Yaiche, A.; Coutancier, D.; Rousset, J.; Collin, S. Optical Characterizations and Modelling of Semitransparent Perovskite Solar Cells for Tandem Applications. In Proceedings of the 36th European Photovoltaic Solar Energy Conference and Exhibition, Marseille, France, 9–13 September 2019; Volume 36, pp. 757–763. [[CrossRef](#)]
35. Heidarzadeh, H.; Rostami, A.; Dolatyari, M.; Rostami, G. Plasmon-enhanced performance of an ultrathin silicon solar cell using metal-semiconductor core-shell hemispherical nanoparticles and metallic back grating. *Appl. Opt.* **2016**, *55*, 1779–1785. [[CrossRef](#)] [[PubMed](#)]
36. Zhou, D.; Zhou, T.; Tian, Y.; Zhu, X.; Tu, Y. Perovskite-Based Solar Cells: Materials, Methods, and Future Perspectives. *J. Nanomater.* **2018**, *2018*, 1–15. [[CrossRef](#)]
37. Lee, K.-M.; Lin, W.-J.; Chen, S.-H.; Wu, M.-C. Control of TiO₂ electron transport layer properties to enhance perovskite photovoltaics performance and stability. *Org. Electron.* **2020**, *77*, 105406. [[CrossRef](#)]
38. Liu, W.; Ma, H.; Walsh, A. Advance in photonic crystal solar cells. *Renew. Sustain. Energy Rev.* **2019**, *116*, 109436. [[CrossRef](#)]
39. Tanabe, K. A Review of Ultrahigh Efficiency III-V Semiconductor Compound Solar Cells: Multijunction Tandem, Lower Dimensional, Photonic Up/Down Conversion and Plasmonic Nanometallic Structures. *Energies* **2009**, *2*, 504–530. [[CrossRef](#)]
40. Hörantner, M.T.; Zhang, W.; Saliba, M.; Wojciechowski, K.; Snaith, H.J. Templated microstructural growth of perovskite thin films via colloidal monolayer lithography. *Energy Environ. Sci.* **2015**, *8*, 2041–2047. [[CrossRef](#)]
41. Chen, H.; Zhu, W.; Zhang, Z.; Cai, W.; Zhou, X. Er and Mg co-doped TiO₂ nanorod arrays and improvement of photovoltaic property in perovskite solar cell. *J. Alloy. Compd.* **2019**, *771*, 649–657. [[CrossRef](#)]
42. Meng, K.; Gao, S.; Wu, L.; Wang, G.; Liu, X.; Chen, G.; Liu, Z. Two-Dimensional Organic–Inorganic Hybrid Perovskite Photonic Films. *Nano Lett.* **2016**, *16*, 4166–4173. [[CrossRef](#)]